Phosphorescent-based pavements for counteracting urban overheating – A proof of concept

Ioannis Kousis[a], Claudia Fabiani[a,b], Laura Gobbi[a], Anna Laura Pisello[a,b,*]

[a] CIRIAF - Interuniversity Research Center, University of Perugia, Via G. Duranti 67, 06125 Perugia, Italy
[b] Department of Engineering, University of Perugia, Via G. Duranti 97, 06125 Perugia, Italy

ABSTRACT

The built environment is particularly sensitive to elevated temperatures across urban areas. Furthermore, engineered materials usually amplify surface overheating, exacerbating urban heat island and cooling energy needs. In the last decades, the scientific community introduced a new class of materials, i.e. cool materials, in the attempt of mitigating these phenomena. In this context, this work investigates the hygrothermal and radiative potential of phosphorescent-based paving solutions and benchmarks their performance against commercially available cool concrete. To this end, an extensive outdoor monitoring campaign was carried out in terms of surface/air temperature, relative humidity, reflected solar radiation and wind speed/direction during summer 2019. Phosphorescent-based fields were found to maintain lower superficial temperature than the reference during the hottest hours of the day, by up to 0.9 °C and 3.3 °C in terms of average and absolute values, respectively. Even though other cooling techniques have been found to have higher cooling effect, the outcomes of this study, reveal for a first time, (i) the promising thermal behavior of phosphorescent-based pavements, as well as (ii) their potential for developing advanced cool materials equipped with both radiation reflection and re-emission mechanisms.

1. Introduction

Over the past decades, rapid urbanization led to significant modifications of urban surfaces. Natural land is continuously converted to urban land (Nurwanda and Honjo, 2020) and the local surface energy balance is altered. As a result, elevated surface and ambient temperatures plague urban areas all around the world (Yun et al., 2020). In particular, the effect of urban overheating in contrast with the cooler rural surroundings, also known as the urban heat island (UHI) phenomenon, is widely considered as an epoch-making repercussion of human-induced activities (Mathew et al., 2019; Cosgrove and Berkelhammer, 2018). UHIs are acknowledged to pose a severe threat to human health (Walter and Gibson, 2020). In fact, urban warming is related to negative health outcomes, such as morbidity and mortality, especially when a heat wave occurs simultaneously (Pyrgou et al., 2017). This is all the more important considering that urban residents comprise more than half of the world's population (World Bank, 2018).

Additionally, UHI is highly interlinked to amplified cooling loads during summer period (Vardoulakis et al., 2013). Energy demand is further increased by the unceasing urban sprawl, population growth, and infrastructure expansion (Fichera et al., 2016). Such an increase in energy demand, in turn, implies higher carbon dioxide (CO_2) emissions that further boost climate change both at local and global scale (Radulovic et al., 2011).

Given the complexity of the urban systems, the corresponding microclimatic context is diverse and therefore its buffers are numerous (Steeneveld et al., 2014). The thermal properties of the building envelope and paved surfaces alongside the arisen local-scale flows, are the dominant components of the urban fabric (Ferguson, 2005; Roth, 2000). Specifically, as proposed elsewhere, pavements, either roads or sidewalks, may cover more than 40% of the overall cities' area (Santamouris, 2013). The materials however that have been implemented by the pavement industry so far are highly prone to absorb and store radiation energy (Doulos et al., 2004; Qin and Hiller, 2014).

Moreover, on a practical side, paving systems are usually complemented by artificial lightning sources. Outdoor artificial lightning systems are apparent in most of urban areas mainly for providing or enhancing vision and accessibility. Outdated lighting installations however, produce excessive energy consumption possibly amplifying the environmental footprint of cities and their effect in terms of UHI (Clinton and Gong, 2013).

Mitigating the factors that intensify UHI is a multi-faceted

---

* Corresponding author.
  E-mail address: anna.pisello@unipg.it (A.L. Pisello).

challenge. On that account, various techniques have been reported and implemented as UHI countermeasures (Koc et al., 2018; Ulpiani, 2019; Zhu and Mai, 2019). Developing cool pavements is a well-reported mitigation strategy. Cool pavements are typically divided in two main categories; (i) reflective and (ii) evaporative pavements. The former decrease the solar gains and hence the local surface temperature due to high infrared emittance and solar reflectance (SR), i.e. high albedo, while the latter retain water and remain cooler due to evaporative cooling (Qin, 2015a).

In particular, increasing the albedo of a surface has been reported as a promising strategy for decreasing both surface and air temperature in the built environment. A recent study of Santamouris et al. (2017) evaluated several large-scale mitigation strategies concerning the implementation of cool paving material in the built environment. Results showed a peak air temperature drop of 2.5 °C. Kolokotsa et al. (2018) replaced conventional pavements with cool paving stones in a neighborhood in Athens, Greece, reducing surface temperature by almost 10 °C. The corresponding decrease of air temperature was 0.3 °C at 2 PM. Similarly, Santamouris et al. replaced 4500 m² of conventional paving materials with light yellow colored cool ones. They reported a drop of peak air and surface temperature of 1.9 °C and 12 °C, respectively (Santamouris et al., 2012). In another large scale study by Kyriakodis and Santamouris (Kyriakodis and Santamouris, 2018), a reduction of 11.5 °C and 1.5 °C in terms of surface and air temperature, was reported upon the installation of cool asphalt and photocatalytic concrete. Despite the acknowledged beneficial effect of these solutions, implementing white or light colored surfaces is sometimes unreasonable due to esthetic or cultural reasons. In this context, Rosso et al. (2017) developed cool-colored mortars with solar reflectance around 0.7 and demonstrated a surface temperature drop of 8 °C with respect to their non-cool counterparts. Towards this direction, Berdahl et al. (2016) suggested that even higher performance can be succeeded by exploiting materials with photoluminescent properties. In photoluminescent materials, the absorbed photons are, indeed, partly re-emitted as visible light, rather than long-wave radiation. Therefore, they can complement the cooling potentiality of high albedo materials with the additional quality of photoluminescence, in a twofold solar rejection mechanism defined as Effective Solar Reflectance (ESR) (Garshasbi and Santamouris, 2019). As evidence, Berdahl et al. spread a layer of synthetic ruby crystals on a white surface to obtain a red coating with 6.5 °C lower surface temperature in the sun compared to conventional red materials.

In more detail, the energy balance of a classic material either conventional or cool is defined according to Eq. (1):

$$R_n = S_\downarrow + L_\downarrow - S_\uparrow - L_\uparrow \tag{1}$$

where R_n is the net radiation gains of the surface, S and L are the shortwave and longwave radiative components respectively and the upward/downward arrows identify upwelling/downwelling components. Eq. (1), considering the reflection and emission capability of a surface, can be written in the following form:

$$R_n = S_\downarrow + L_\downarrow - (a_{SW} \cdot S_\downarrow) - (a_{LW} \cdot L_\downarrow + \epsilon \sigma T^4) \tag{2}$$

where the factor a_{SW} is the reflectance (or albedo) of the surface in the shortwave range, a_{LW} is the reflectance (or albedo) of the surface in the longwave range, and ϵ is the thermal emittance of the surface.

In photoluminescent materials, an extra factor of emissivity must be introduced in the shortwave an near infrared range because of their capability to reemit part of the absorbed radiation in the visible and near infrared part of the spectrum:

$$R_n = S_\downarrow + L_\downarrow - (a_{SW} \cdot S_\downarrow + \epsilon_{SW} \sigma T^4) - (a_{LW} \cdot L_\downarrow + (\epsilon_{LW} + \epsilon)\sigma T^4) \tag{3}$$

where the factors ϵ_{SW} and ϵ_{LW} represent the additional emittance in the shortwave and in the near infrared range and characterize the ESR of a phosphorescent material. All this considered, further exploitation of photoluminescent properties might yield breakthroughs towards UHI

mitigation (Berdahl et al., 2016).

Phosphorescent materials are a subcategory of photoluminescent materials that emit light due to a precedent absorbance of photons. In this case, the emitted light is a result of a spin-forbidden process, through which the radiative decay of the excited electrons takes place within different spin multiplicity states (Ceroni, 2016). Therefore, the emitted radiation in form of light can persist for a long period; from seconds up to a couple of days. Given this merit, phosphorescent materials have been utilized as an alternative form of lightning system. Road signs, house paths, biking routes, exit routes and parking lots are the most common implementations of these materials. Despite the use of phosphorescent surfaces may enhance visibility, accessibility and security perception, a small number of studies has focused on their application to the paving infrastructure as an alternative form of artificial lighting (Praticò et al., 2018; Gutiérrez and Colorado, 2020). Additionally, to the best of the authors' knowledge, despite their unique ESR property, phosphors' radiative and hygro-thermal properties have been overlooked, so far. This is all the more surprising since an apt fit of ESR into urban components may enhance their solar rejection without compromising the intrinsic properties, such as solar reflectance, of the hosting agent either it is conventional or cool.

This study, acknowledging the well reported intrinsic lighting properties of phosphorescent materials, aims, for the first time, to make use of phosphors properties as a counteracting system for tackling UHI incidences. To that end, an extensive in-field monitoring campaign was carried out in central Italy, within a dedicated facility designed for UHI-mitigating skins during the summer period. Specifically developed phosphorescent-based paving surfaces exposed to real meteorological conditions were multi-variously investigated over their hygro-thermal and radiative qualities and benchmarked against a conventional concrete counterpart. The main metrics of UHI intensity, i.e. surface/ambient temperature, relative humidity, albedo value and reflected solar radiation, of five different phosphorescent materials were obtained throughout the months of July and August. At last, a critical evaluation of the results and future targets for this novel UHI mitigation urban component are further discussed.

2. Methodology

2.1. Pilot plant

In this work, an in-field experimental investigation of phosphorescent-based paving fields in terms of radiative and hygro-thermal behavior under real life varied microclimatic conditions was carried out. To this purpose, a specifically designed pilot plant was developed and a multi-variable experimental campaign was conducted. The pilot plant comprised five paving fields equipped with different types of phosphorescent materials, and a reference application produced using a common cool-concrete solution. The monitoring campaign was carried out within the summer months of July and August, i.e. the warmest months for the region during an annual circle. In the following, the main characteristics of the installed pavements are presented and the monitoring campaign is described in details. The experimental fields were developed in a specifically designated site in Perugia University (SURBEX installation). The area of the monitoring campaign was chosen so as to be (i) fully uncovered from the adjacent buildings' shadow and (ii) hardly accessible to laymen.

2.1.1. Description of the phosphorescent components

Two different types of phosphorescent components were used in this work: (i) glass grits and (ii) epoxy-based glazes. In more detail, a yellow glass grit and a blue glass grit (see Fig. 1a) with a maximum diameter of 3 cm were used in partial replacement of the aggregates in the concrete mix design. A coarse and a fine-grained glaze, were sprayed on top of the external surface of the draining concrete upon curing. The glazes were produced by mixing phosphorescent glass grits with a maximum
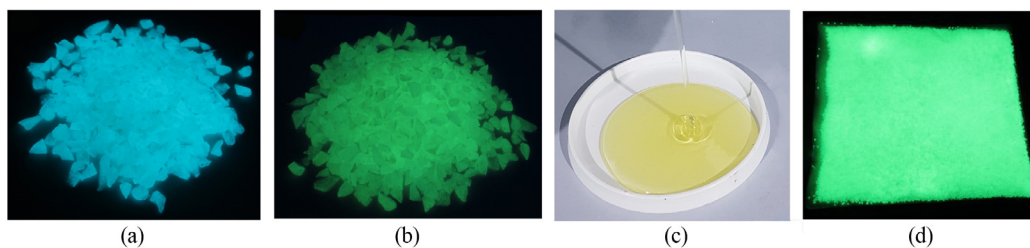
Fig. 1. Phosphorescent materials used in the SURBEX installation: (a) yellow glass grit (used in field 1 and 3), (b) blue glass grit (used in field 2 and 3), (c) epoxy resin used for producing the phosphorescent glaze (used in field 4 and 5), and (d) fine glass aggregates with a 0.2 cm diameter, used for the production of the fine-grained glaze (used in field 4). (For interpretation of the references to colour in this figure legend, the reader is referred to the web version of this article.)

diameter of 1 cm (coarse-grained glaze, see Fig. 1b) and 0.2 cm (fine-grained glaze, see Fig. 1d) with an epoxy resin for external finishing applications (see Fig. 1c). All the phosphorescent components are based on strontium aluminate with dysprosium and europium dopants (characterized by the chemical formula $SrAl_2O_4$: Eu^{+2}, Dy^{+3} in the case of the yellow pigment and $Sr_4Al_14O_25$: Eu^{+2}, Dy^{+3}, B^{+3} for the blue one).

2.1.2. Description of the fields

The phosphorescent materials presented in Section 2.1.1 were integrated in a conventional light-colored concrete mix design and in a draining concrete for producing five novel paving fields equipped with a phosphorescent capacity. The same amount of additions was used in each application, i.e. 300 kgm^{-2}, taking into account the economic feasibility of the pavements which were produced using existing components already in the market. Additionally, a sixth field purely made of conventional light-colored concrete was also produced for comparison purposes. The main characteristics of each field are listed below:

1. Reference field – conventional light-colored concrete (see Fig. 2d);
2. Field 1 – yellow phosphorescent grits embedded in conventional light-colored concrete (see Fig. 2e);
3. Field 2 – blue phosphorescent grits embedded in conventional light-colored concrete (see Fig. 2f);
4. Field 3 – blue and yellow phosphorescent grains embedded in conventional light-colored concrete (see Fig. 2g);
5. Field 4 – phosphorescent fine-grain glaze sprayed on top of the dark

draining concrete (see Fig. 2h);
6. Field 5 – phosphorescent coarse-grain glaze sprayed on top of the dark draining concrete (see Fig. 2i).

As represented in Fig. 2, each field consists of at least three layers: a subgrade from the existing ground, a 13 cm-thick layer of permeable aggregates, and the 10 cm-thick concrete layer (either conventional light colored or draining concrete). The phosphorescent grits are introduced in the last 2 cm of this layer in fields 1, 2, and 3. Fields 4 and 5, finally, which are made of draining concrete, present an additional stratum of superficial phosphorescent glaze. The concrete platforms were developed above the 13 cm-thick permeable aggregate layer with their sides exposed to air using a wooden frame to separate the fields from each other and minimize eventual lateral heat losses.

Following the corresponding standards (ASTM, 2006), each of the developed fields covers a total area of 4 × 4 m. The concrete utilized for the formulation of all the fields is commercially available and indicated for the development of pavements (more details are reported in Table 1). The cements at the base comply with the current standards UNI EN 197-1 (EN 197-1, 2011) and UNI EN 197-2 (EN 197-2, 2014), while their additives which respect UNI EN 934-2 (EN 934-2, 2012), help reaching the pre-set mechanical resistance. A schematic representation of the fields is given in Fig. 1a.
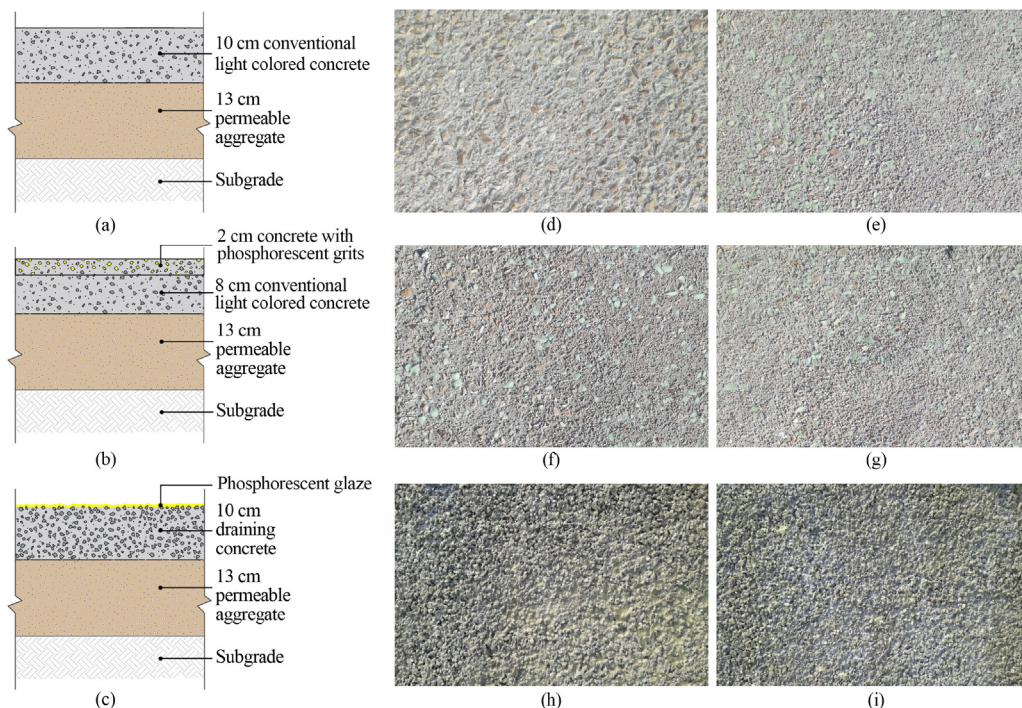

Fig. 2. On the left – schematic representation of the layers that characterize the different fields produced in the SURBEX installation at Perugia University for (a) the reference field, (b) field 1, 2 and 3, and (c) field 4 and 5. On the right – pictures of the different fields: (d) reference field, (d) field 1, (f) field 2, (g) field 3, (h) field 4, and (i) field 5.

Table 1
Technical characteristics, i.e. characteristic compressive strength (Rck), consistency class (CC), density (ρ), water flow rate (Q_w), and maximum diameter of the aggregates (ϕ_{max}), of the concretes used in the investigated fields (Colabeton, 2018a; Colabeton, 2018b).

Concrete	Rck (MPa)	CC	ρ (kg m^{-3})	Q_w (l m^{-2} min^{-1})	ϕ_{max} (mm)
Conventional light-colored	30–45	S3/S4	2350[a]	–	15–25
Draining	15–20	S1	1600–2000	100–350	10–15

[a] Measured by authors.

2.2. In-field monitoring

An extensive monitoring campaign of identical in-situ measurements was performed for the six developed fields and is still ongoing. Although, for the purpose of this work, only the period from July 22 to August 29, 2019 (characterized by the maximum values of solar radiation and hence solar gains), was selected and analyzed. The hygro-thermal and the radiative behavior of each field was accurately monitored, together with the most important local boundary conditions.

2.2.1. Monitoring of the microclimatic boundary conditions

In order to capture and evaluate the overall microclimatic background boundary conditions, an outdoor monitoring setup located over the building roof of the same premise was utilized (see Fig. 3b). The roof monitoring set-up includes a weather station measuring air temperature, wind speed and direction, relative humidity and incoming solar radiation. All the sensors perform a continuous monitoring campaign collecting data every 10 s and producing average values every 10 min (Pisello et al., 2017). The recorded data are gathered via a connected Data Logger station which is coupled with a web-based platform wherein the sensors' data become available for download.

2.2.2. Monitoring of the radiative behavior

Capturing the radiative profile allows to determine its capacity to reflect solar radiation, and consequently, its albedo. Two different ASTM standard testing methods have been reported for calculating solar reflectance of a surface: ASTM C1549 (ASTM, 2009) and ASTM E1918 (ASTM, 2006). The former is suited for measurements over flat and homogeneous smooth surfaces while the latter can be used in all types of plane surfaces. Further methods, such as the mask-free method for smaller scale monitoring have been reported (Qin et al., 2018).

The investigated fields were specifically designed to follow the methodology of ASTM E1918 (ASTM, 2006), except one unique value of incoming solar radiation was measured and later used for the albedo calculations, i.e. the one from the meteorological station in Section 2.2.1. Each field was equipped with a South-oriented pyranometer facing its surface. The pyranometer was fixed on a 0.5 m-long arm adjusted on an aluminum pole in order to face the center of the field at a height of 0.5 m (see Fig. 3c). Using this equipment, the reflected shortwave radiation (SR) was continuously measured and average data were registered with a constant time-step of 10 min. Consequently, the obtained data were utilized for reckoning the albedo profile of each field in the time range 10 AM – 2 PM LST. The technical characteristics of the described pyranometer can be found in Table 2.

2.2.3. Monitoring of the hygro-thermal behavior

Capturing the hygro-thermal profile of a surface is essential for evaluating its interaction with the urban environment. To this aim, in this work, superficial temperature, air temperature and relative humidity were continuously monitored for each field. Additionally, the air velocity profile of the area was also measured in close proximity of the fields (at a distance of about six meters, as reported in Fig. 3a to avoid drop shadows on the investigated surfaces). As in the above for the meteorological and radiative monitoring, average data were collected with a time step of 10 min. In more detail, each field was equipped with a superficial temperature sensor, installed on the internal corner of a

fictitious 1×1 m square with two edges overlapping the north and east outer borders of each field. This particular position was selected in order to (i) minimize any influence on the concurring measurements of the reflected radiation and (ii) minimize the effect of lateral thermal disturbance. Air temperature and relative humidity profiles were also continuously monitored at the center of each field (the sensors were clamped at the same support of the pyranometer, as shown in Fig. 3c) at a height of 0.5 m to verify the extinguishing of the superficial effect. The air velocity profile was measured at the same height to quantify the effect of wind speed and direction of the extinguishing effect.

Two different types of mobile appliances were used for the reported monitoring campaign; (i) Tiny-tag data loggers and (ii) a National Instrument wireless sensor network (NIWSN). In particular, two different versions of free-standing Tiny-tags were implemented for the monitoring campaign. A Tiny-tag data logger with a built-in probe, for measuring air temperature and relative humidity and a Tiny-tag data logger with a built-in probe for measuring surface temperature. The NIWSN was also equipped with superficial temperature sensors, air temperature and relative humidity sensors, and a wind speed and direction sensor. Every kind of equipment, i.e. surface temperature, air temperature and relative humidity sensors, were firstly calibrated within the controlled environment of a climatic chamber (ATT DM 340 SR from Angelantoni Test Technology (Angelantoni Test Technologies, 2012)) in order to guarantee the comparability of the obtained results. The technical characteristics of all sensors are tabulated in Table 2.

3. Results

In this section, the results from the outdoor in-field monitoring campaign are presented. In particular, the obtained monitored profiles were post-processed in order to define the average behavior of each field in a representative sunny and cloudy day in Summer condition in central Italy. The average sunny day is calculated by taking into account all the days characterized by a substantially clear sky condition. The average cloudy day, on the other hand, was calculated considering all the days characterized by a substantially cloudy sky condition. Sunny and cloudy days were distinguished considering the threshold of 500 Wm^{-2} as the maximum average daily insolation for the light ours in cloudy days and the minimum one for sunny days. This specific threshold was selected based on the authors' experience from long term outdoor monitoring, considering the maximum and the minimum insolation level at our latitude in summer. Additionally, the obtained surface, air temperature and the relative humidity profiles characterizing the different fields during three representative sunny (August, 3–5) and cloudy (July, 27–29) days were also compared for better investigating the differences among them.

3.1. Meteorological background

3.1.1. Ambient temperature

The overall ambient temperature in the implementation area can be seen in Fig. 4. The monitoring period is characterized by high values of dry bulb temperature during the daytime, e.g. maximum recorded temperature equals to 37.6 °C and average temperature equals to 25 °C. The overall temperature profile exceeds the typical average regional ambient temperature profile reported in the Appendix A. Thus it can be
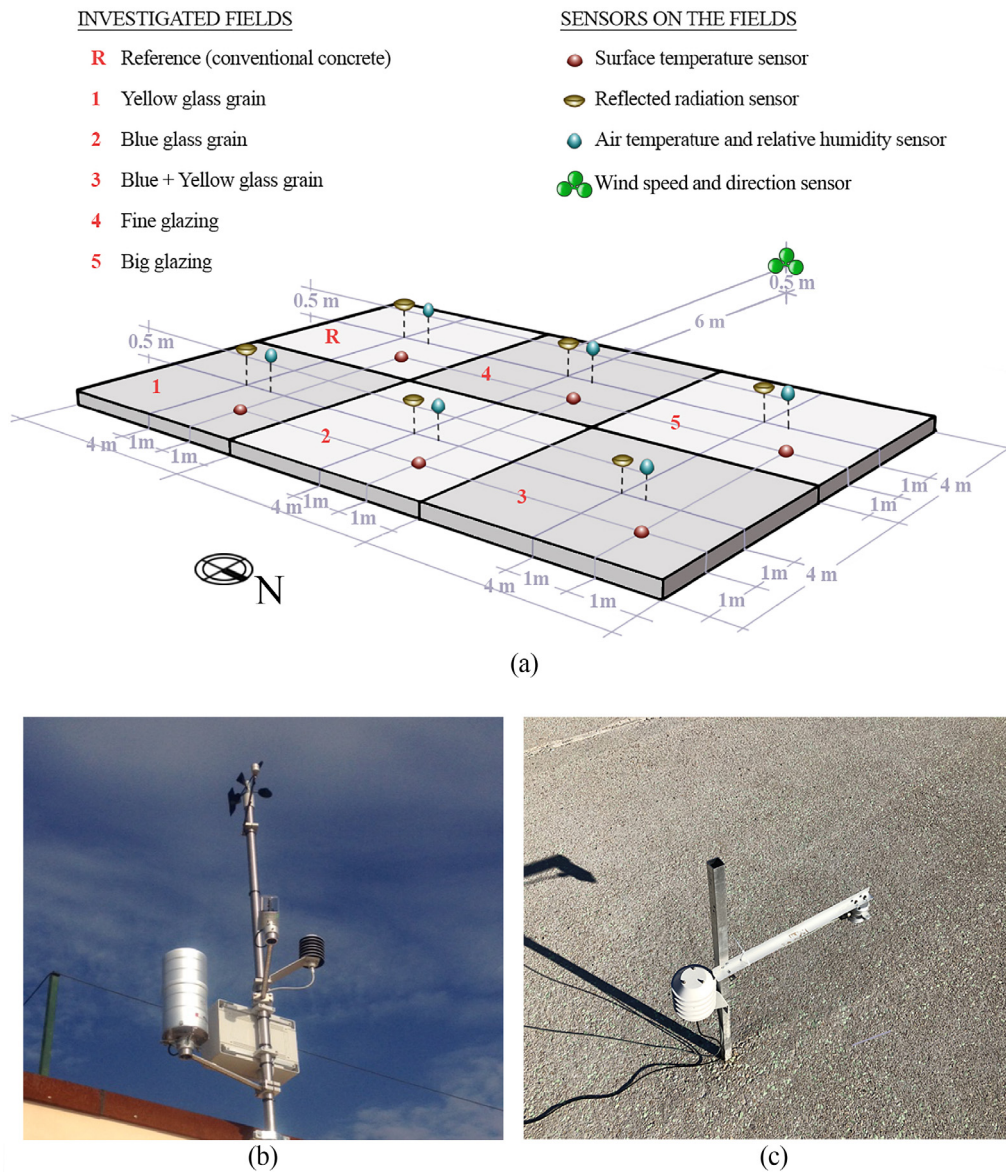
INVESTIGATED FIELDS

R Reference (conventional concrete)
1 Yellow glass grain
2 Blue glass grain
3 Blue + Yellow glass grain
4 Fine glazing
5 Big glazing

SENSORS ON THE FIELDS

● Surface temperature sensor
● Reflected radiation sensor
● Air temperature and relative humidity sensor
🍀 Wind speed and direction sensor

(a)

(b)

(c)

Fig. 3. (a) Schematic representation of the investigated fields and the corresponding sensors, (b) view of the weather station located on the roof of the university building, and (c) view of the monitoring setup on field 2.

Table 2
Characteristics of the sensors installed in-field.

| Sensor	Producer	Model	Principle	Range	Accuracy	Location	Acquisition
Reflected Radiation	LSI Lastem	DPA 053	Thermopile	0–2000 W m^{-2}	5% (daily totals)	0.5 m-height	LSI
	Delta OHM	LP Pyra03	Thermopile	0–2000 W m^{-2}	5% (daily totals)	0.5 m-height	NIWSN
Air temperature	E + E Elektronik	EE 060	Thermoresistor	-40 to 60 °C	±0.3 °C	0.5 m-height	NIWSN
	Gemini	TGP 4500	Thermoresistor	-25 to 85 °C	±0.6 °C @ (0–40 °C)	0.5 m-height	Tinytag
Relative humidity	E + E Elektronik	EE 060	Capacitive sensor	0–100%	$\pm2.5\%$ @ (-15 to 40 °C)	0.5 m-height	NIWSN
	Gemini	TGP 4500	Capacitive sensor	0–100%	$\pm3\%$ @ (25 °C)	0.5 m-height	Tinytag
Surface temperature	Metron	PT100 3-wire	Thermoresistor	$-200 - 500$ °C	±0.5 °C @ (-10 to 85 °C)	On the surface	NIWSN
	Gemini	TGP 4017	Thermoresistor	-45 to 85 °C	±0.6 °C @ (0–40 °C)	On the surface	Tinytag
Wind speed	Robinson	VV1	Magnetic trasducer	0.28–50 ms^{-2}	±0.1 ms^{-2} @ (0.4–30 ms^{-2})	0.5 m-height	NIWSN
Wind direction	Robinson	DV 4017	Hall sensor array	0–360 °	±2 °	0.5 m-height	NIWSN
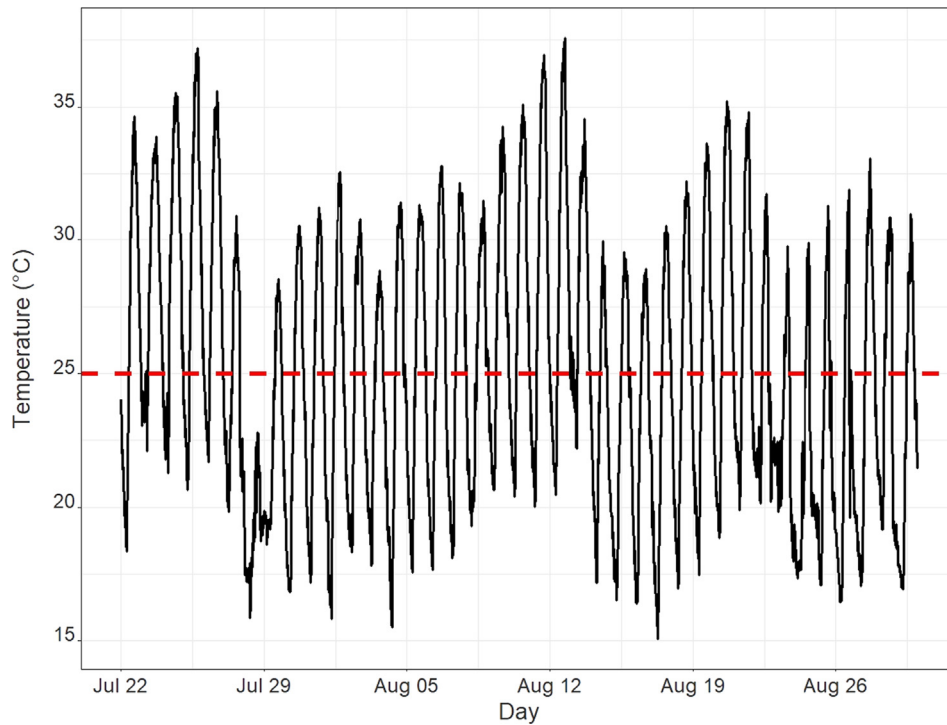
Fig. 4. Ambient temperature profile within the monitoring period.

considered (i) as representative of a hot summer period and (ii) ideal conditions for investigating the UHI mitigation potential of the applied urban pavement materials. Additional data representing the meteorological background in the period under investigation are reported in the Appendix.

3.2. Radiative behavior

Fig. 5 illustrates the reflected solar radiation profile of the investigated fields for the three selected representative sunny and cloudy days. Fields 4 and 5 clearly show the worst reflectance capability in
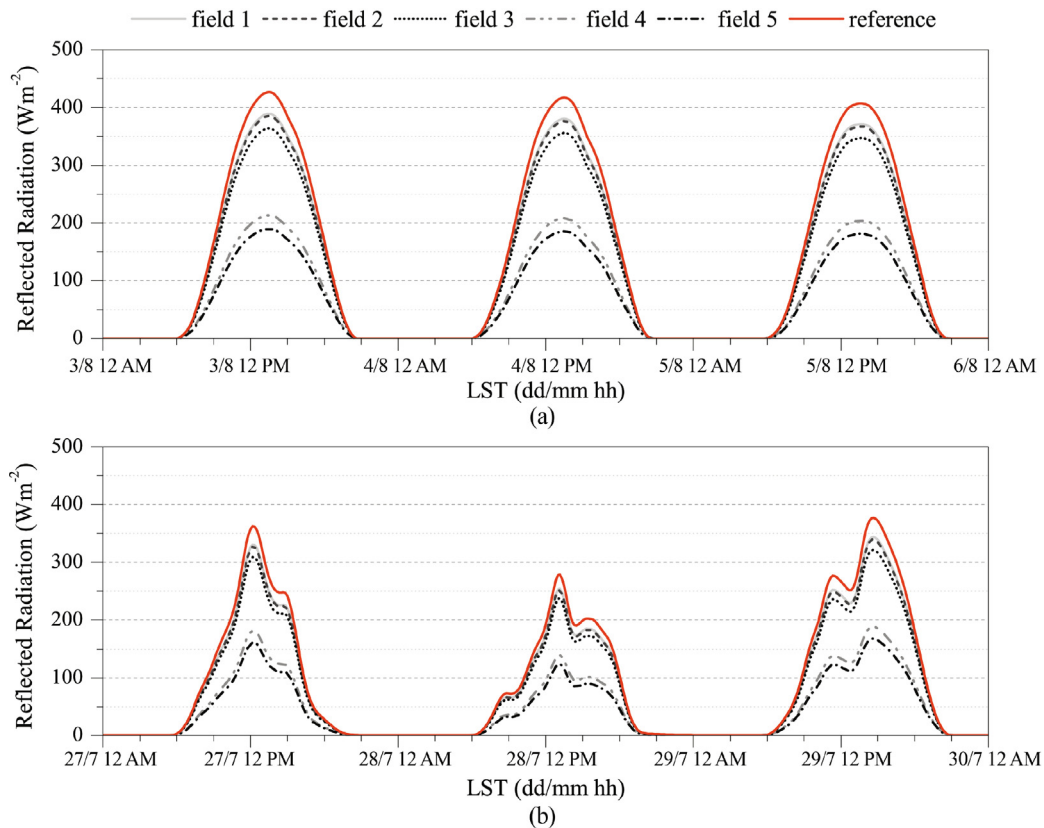
Fig. 5. Reflected solar radiation of all fields during the selected representative (a) sunny and (b) cloudy days.
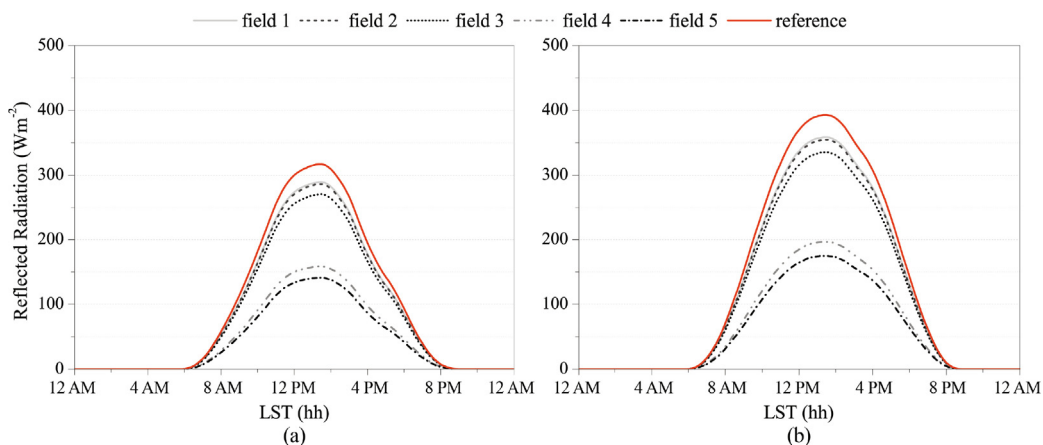
Fig. 6. Reflected solar radiation of all fields during the average (a) sunny and (b) cloudy days.

both cases, while the reference field is always associated to best reflectance performance, closely followed by field 1, 2, and 3. This is on the one hand imputable to the specific kind of concrete used in the fields, and on the other one, to the difference in surface roughness between the applications. Reference field and fields 1, 2 and 3 are, indeed, all made of conventional light-colored concrete, while field 4 and 5 are both made of a darker and permeable concrete matrix showing a highly irregular surface due to the huge number of voids that characterize its outer layer.

The introduction of the phosphorescent additions as glass grits allows to preserve the cool reflectance capability of the light-colored concrete. Better performance seem to be obtained by the use of one unique type of aggregate, either yellow or blue, although the difference among the applications is almost negligible. Focusing our attention on fields 4 and 5, the fine-grain glaze always shows higher reflectance capability if compared to the coarse-one. This suggests that the introduction of a more uniform layer produced with a finest material allows to maximize the phosphorescent phenomenon. Results from the average solar reflectance profiles (see Fig. 6) of the fields calculated in cloudy and sunny conditions perfectly replicate the ones from the representative days on the above. However, as expected, more uniform bells are depicted in this case.

Table 3 presents the average albedo value of all fields, calculated in the time range between 10 AM and 2 PM LST by using the incoming solar radiation from the meteorological station. Reference together with fields 1, 2, and 3 shows albedo values well above 0.3, i.e. comparable to existing high-reflectance concrete solutions in the literature (Li et al., 2013; Castaldo et al., 2015). The introduction of the phosphorescent glaze, on the other hand, allows to obtain albedo values as high as 0.17 in the case of the coarse-grain application and 0.19 in the case of the fine-grain one, despite using a relatively dark and porous matrix. This suggests that the addition of phosphorescent materials into a conventional dark material may enhance its ESR.

3.3. Hygro-thermal behavior

3.3.1. Superficial temperature

Fig. 7 shows the superficial temperature profiles of the investigated fields over the three representative sunny days. As expected, fields 4 and 5, characterized by a significantly lower albedo, always show

higher surface temperatures than the reference. Differences as high as 7 °C can be found around 3 PM, when the solar heat gains reach the peak. Field 4, in particular, despite the higher albedo compared to field 5 reaches the highest temperature values. This suggests a worse interaction between the resinous fine-grain phosphorescent composite and the permeable application compared to the coarse-one. More in detail, the fine-grain glaze probably produces a reduction in the number of open cavities in the concrete matrix, significantly reducing the evaporative cooling effect. This, however, appears less evident in the case of the coarse-grain solution which despite being associated to higher solar gains allows to maintain significantly lower surface temperatures compared to the fine glaze.

Concerning fields 1, 2, and 3, results show that the introduction of the phosphorescent aggregates in the conventional light-colored concrete maintains the already positive thermal response of the reference. Furthermore, a non-negligible time delay with respect to the reference (up to 55 min lag is found for field 3 in August, 3) allows these fields to maintain lower surface temperatures during the morning and the early afternoon. Conversely, higher temperatures are registered later in the afternoon and during the night, when however, lower wind speeds reduce convective contribution to heat dissipation (see Fig. 7b).

Fig. 8 depicts the surface temperature profiles of the tested fields during the representative cloudy days. In this case, also due to the highest registered wind speeds, no significant differences are usually found among the different profiles. The only exception is represented by field 4, which once again results in the highest surface temperature values all day long. It is noteworthy, however, how the introduction of the phosphorescent materials seems to maintain a more stable profile in the central hours of the day, particularly on July, 28, when temperatures differences as high as 2.7 °C can be found among the reference and the phosphorescent fields. Additionally, also in this case, a general peak temperature delay can be found in all the innovative fields, confirming the idea that phosphorescence could produce a time lag in the superficial thermal response of the fields.

Results from the average cloudy and sunny day are illustrated in Fig. 9. As can be seen, also in this case the darker fields, i.e. 4 and 5, are characterized by the highest temperature values and the difference between them is inversely proportional to the amount of incoming solar radiation. Additionally, further corroborating the positive effect identified in the above, fields 1, 2, and 3 show lower skin temperatures compared to the reference during the morning and the early afternoon. A maximum difference of about 3.4 °C can be found in the average sunny day between field 1 and the reference, while a peak value of 2.6 °C can be seen in the case of fields 2 and 3. Once more, the highest skin temperatures of the phosphorescent-base fields are always delayed compared to the reference with a time lag varying from 35 min (field 3) to 20 min (field 4) in sunny conditions, and from 95 min (field 3) to
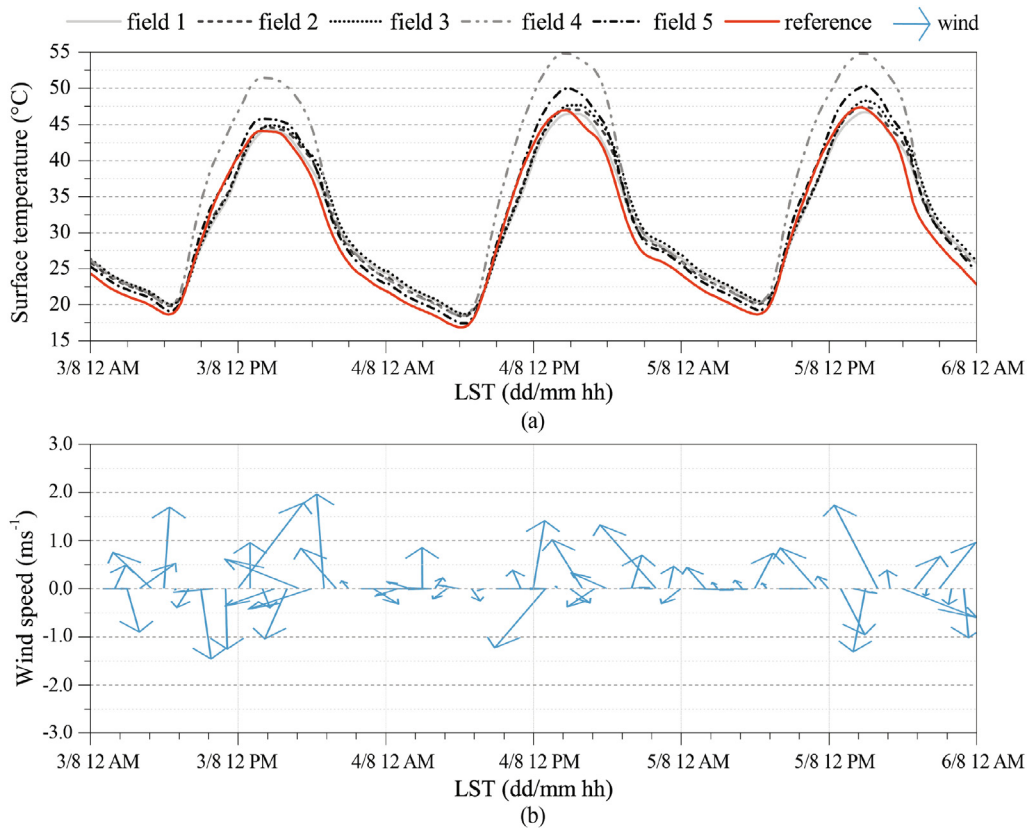
Table 3
Albedo values of investigated fields.

	Field 1	Field 2	Field 3	Field 4	Field 5	Reference
Albedo	0.35	0.35	0.33	0.19	0.17	0.39

Fig. 7. (a) Surface temperature and (b) wind velocity profiles of the investigated fields during the three representative sunny days.
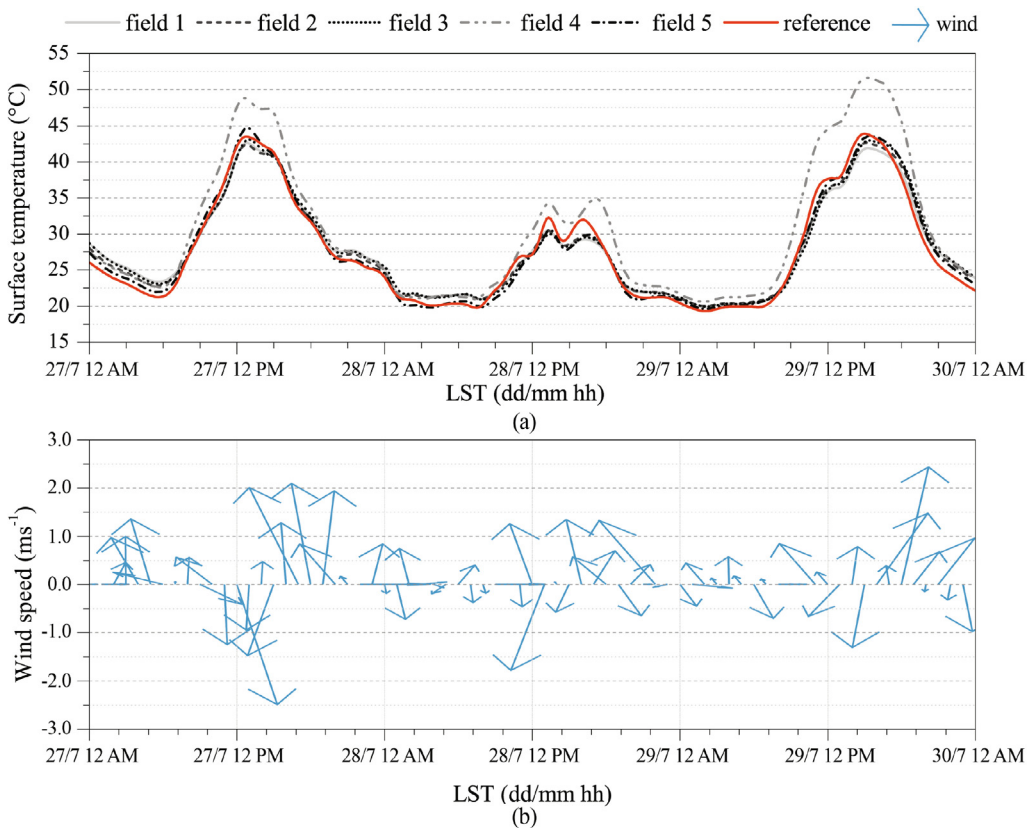

Fig. 8. (a) Surface temperature and (b) wind velocity profiles of the investigated fields during the three representative cloudy days.
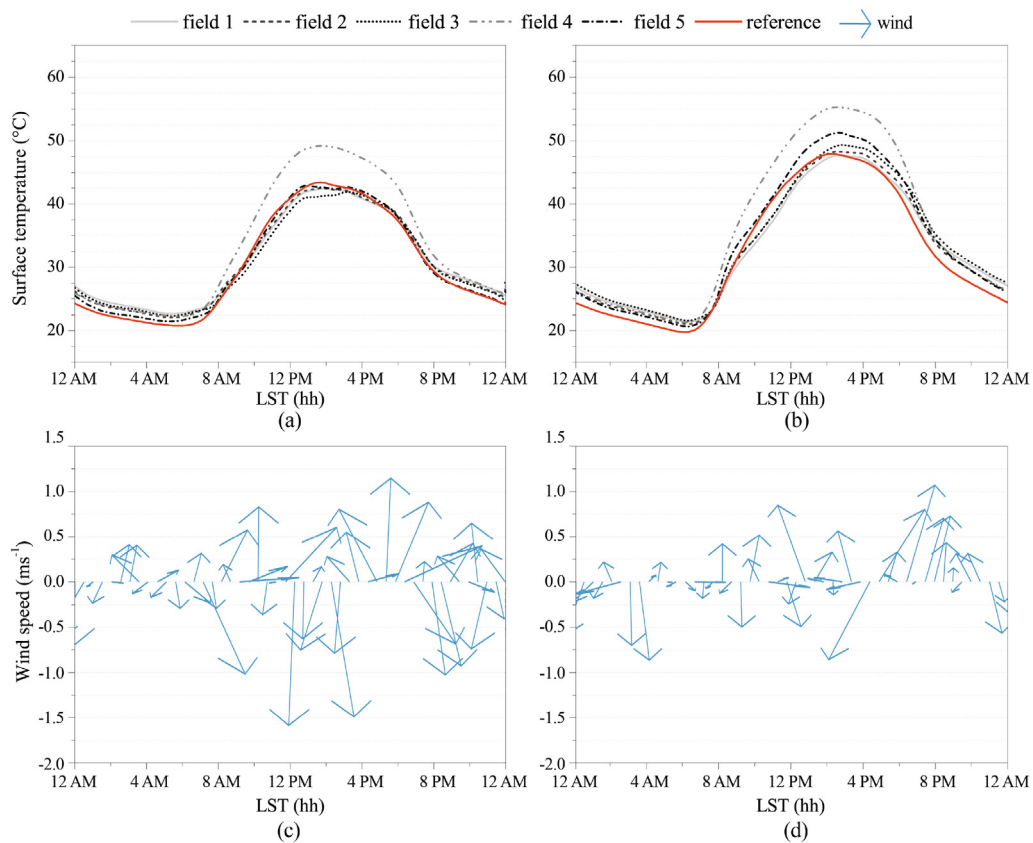
Fig. 9. (a, b) Surface temperature and (c, d) wind velocity profiles for the average cloudy (left) and sunny (right) day.
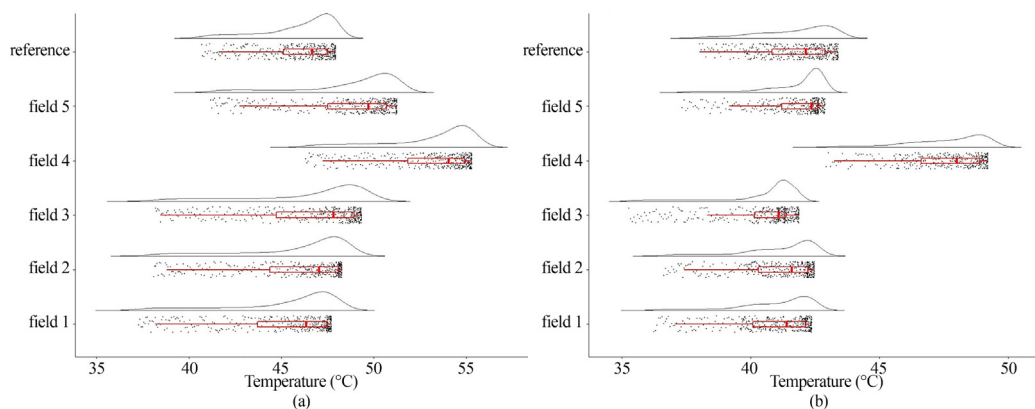

Fig. 10. Rain-plots for average (a) sunny and (b) cloudy day within 11:00 AM 5:00 PM (surface temperature).

10 min (field 2) in cloudy conditions. Finally, also in this case, the reference field is usually associated to lower temperatures during the night and the early morning, i.e. in absence of sun and with reduced wind speeds.

Distribution profiles of the surface temperature from 11:00 AM to 5:00 PM of the average sunny day can be seen in Fig. 10a. As can be seen, the difference between the average temperature registered in fields 1, 2 and 3 and the one of the reference is of about 0.9 °C, 0.7 °C and 1.4 °C, respectively.

Overall, the light colored phosphorescent-based fields 1, 2 and 3 were found to maintain their surface temperature below the reference for a significant fraction of the hot hours of sunny days. This is likely caused by ESR property. Apart from reflecting solar radiation, phosphorescent fields are capable of extra-emitting shortwave radiation, within the visible range. As a result, the twofold rejection mechanism of

solar radiation, i.e. reflection and emission, which is absent in the conventional surfaces (reference field), may further reduce the thermal gains of the surface and hence its surface temperature.

Concerning cloudy days (see Fig. 10b), all phosphorescent based solutions except field 4, were found to have similar (field 5) or lower (fields 1, 2 and 3) superficial temperature compared to the reference throughout the hot hours time frame. In cloudy weather conditions the reduced incoming solar radiation results in reduced thermal gains for all surfaces. Yet, unlike the reference, the phosphorescent-based fields, can still be activated by diffuse solar radiation. Hence they can continuously emit shortwave radiation and further reduce their surface temperature.

This mechanism may also be spotted in the reported delay concerning the peak surface temperature values of the phosphorescent-based fields compared to the reference. The supplementary emission of
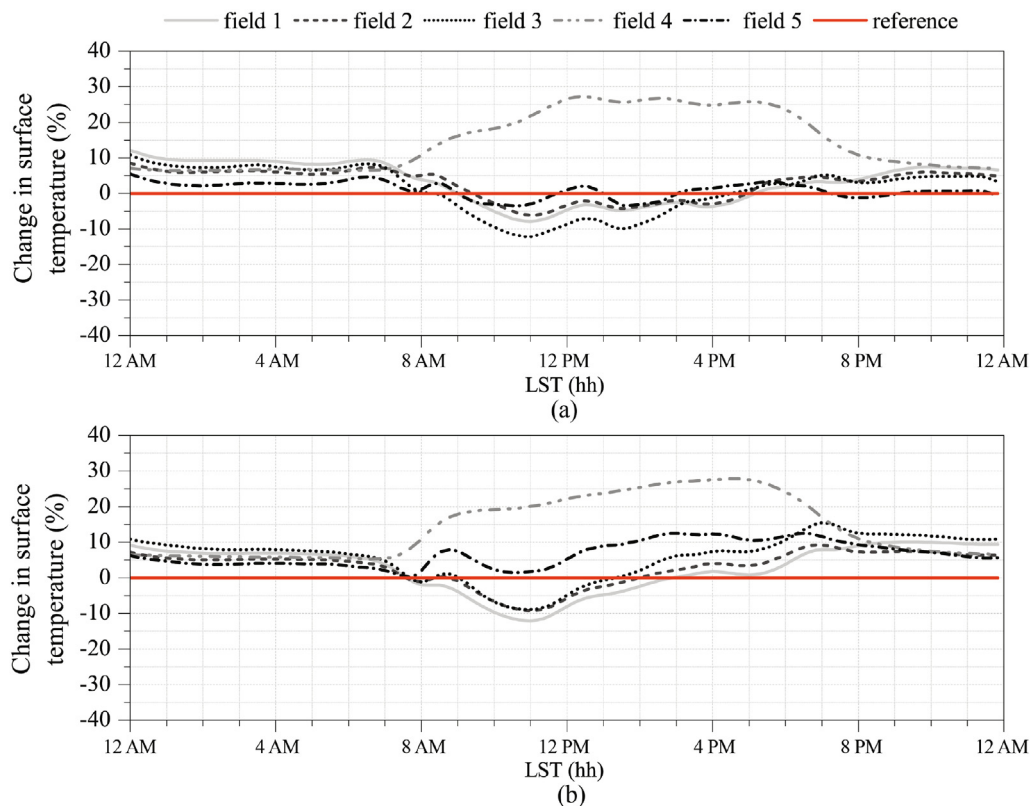
Fig. 11. Change in surface temperature of the considered fields (with i from 1 to 5) during the average (a) cloudy and (b) sunny day, with respect to the maximum surface temperature difference registered in the reference field in the specific day ($T_{field,i}$(t) − T_{ref}(t))/($T_{ref,max}$−$T_{ref,min}$).

shortwave radiation, indeed, can reduce the amount of heat accumulated by the surface. Thus, ESR could be responsible for procrastinating the rise of superficial temperature at pick time, i.e. when mostly needed for outdoors well-being.

3.4. Interpretation of the results

In order to more carefully investigate the effect of the phosphorescent additions on the thermal performance of the fields, we focused our attention on the percentage change in surface temperature, defined as the difference between the surface temperature of the innovative field ($T_{field,i}$(t)) and the reference (T_{ref}(t)), over the maximum surface temperature difference registered in the reference field over the specific average day ($T_{ref,max}$−$T_{ref,min}$). Fig. 11 depicts said variation for the average cloudy and sunny days.

Results demonstrate that field 4 is associated with the highest variations both in sunny and cloudy conditions. The dark colored fine-grain glaze solution shows a peak percentage increase of almost 30% at 12 PM and always above 10% from 8 AM to 8 PM in both cloudy and sunny conditions. The dark colored coarse-grain glaze, on the other hand, shows a better behavior in cloudy conditions (negative variations can be seen between 9 AM and 3 PM in this case), and a general increase in sunny conditions. This is probably due to the combination of the reduced albedo and of the detrimental sealing effect produced by the glaze, particularly the fine one, that probably reduces the evaporative cooling in the draining fields.

Concerning the glass grits fields, all of them show a temperature reduction in the early morning, with temperature variations as high as 10% around 11 PM, but then a slow but unavoidable increase in the slope of the relative variation trend leads to positive values, and thus higher temperatures with respect to the reference, in the afternoon. This effect, which is likely attributed to ESR, is particularly evident in sunny conditions, when peak variations of about 12% and 8% can be

seen around 7 PM in field 3, 1, and 2, respectively. Air temperature and relative humidity were also recorded at a height of 0.5 m above each field. However, the corresponding measurements did not unveil any specific relationship to the different tested fields, not even in very light breeze days. Hence, for brevity reasons, the corresponding graphs were omitted.

Because of economic feasibility, phosphorescent components account for a small fraction of the tested fields, therefore the reflectance of the different surfaces is highly affected by the reflectance quality of the hosting agent, i.e. conventional light colored or draining concrete. The introduction of the phosphorescent additions mostly maintains and even enhances (in the darker applications) the original reflectance of the hosting agent and simultaneously enhances its solar rejection with emission in the shortwave and near infrared spectrum range. In terms of durability, since the main component of all fields is concrete, the final product should maintain the enviable performance of the original mix design. Furthermore, their surface characteristics are easily recovered by simply brushing the external layer due to the specific applications selected for this study, i.e. glass grits and finishing glaze.

4. Concluding remarks

In this work, a novel solution for cool pavements integrating phosphorescent materials was, for a first time, investigated in terms of its radiative and hygro-thermal behavior in order to explore its potential as UHI mitigation strategy for outdoor applications in the built environment. Phosphorescent materials, indeed, are expected to reduce the amount of absorbed shortwave radiation by means of a twofold mechanism: reflectance in the shortwave and additional emittance in the visible and near infrared spectrum range. As a result, phosphorescent-based pavements can naturally contribute towards decreased levels of energy consumption for lightning applications in the outdoor. In more detail, five 4×4 m innovative concrete fields including different

types of phosphorescent materials and a reference conventional light colored concrete solution were produced and extensively monitored during the summer period in terms of reflected radiation, surface temperature, air temperature, relative humidity, and wind speed and direction in the outdoors in Italy.

Results showed that the addition of phosphorescent components does not compromise the solar reflectance of the hosting agent, only slightly reducing the solar reflectance performance of the conventional light-colored solution. Instead it produces a non-negligible surface temperature reduction during typical hot summer days both in cloudy and sunny sky conditions. In particular, the reported reductions during the hottest hours of a typical summer sunny day was up to 3.3 °C. Previous studies on cool materials have concluded to higher temperature decrease. Nevertheless, in our study the cool phoshphorescent components account for a rather small fraction of tested fields' surface. Addition of extra phosphorescent components are expected to enhance the cooling effect.

Phosphorescent-based fields were also found to produce a significant time delay in terms of peak surface temperature compared to the conventional concrete surface both in sunny and cloudy sky conditions. This suggests that the phosphorescent-based fields, can be activated by diffuse solar radiation, producing the emission of additional amounts of shortwave and near infrared radiation also when the direct insolation is reduced or absent.

The results of the present study are related to concrete structure. Thus they should not be generalized for other applications, e.g. asphalt. However, the positive outcomes of this work represent a stimulus for further research concerning the optimization of phosphorescent-based materials both in-lab and in-field. Further dispersion techniques together with varied density configurations should be tested in various types of materials either conventional or cool. Additional investigation on the optical properties concerning both reflection and emission is deemed necessary for exploiting the ESR quality and gauging the potentiality of phosphorescent materials in a larger scale, i.e. in terms of Urban Canyon Albedo (Qin, 2015b). Finally, aging, a well reported issue of cool materials (Berdahl et al., 2008), should be evaluated also for phospshorescent-based urban components.

Declaration of Competing Interest

The authors declare that they have no known competing financial interests or personal relationships that could have appeared to influence the work reported in this paper.

Acknowledgment

Appendix A. Description of the site

The pilot plant presented in this study is developed in central Italy (Perugia city). Perugia is located at the very central area of Italy (43°5'N, 12°30'E, 204 m) and is characterized by a humid subtropical climate (Perugia, 2019). According to the Köppen and Geiger classification the area of Perugia is classified as Cfa implying an overall temperate mild with no dry season and constantly moist climate (Beck et al., 2018). On the whole, seasonality in the area of Perugia is deemed moderate. Winter periods are considered generally as mild with precipitation arising from mid-latitude cyclones. Summer periods are typically characterized as warm and humid with substantial amount of rainfall, e.g. thunderstorms. The average high temperature during summer period is 28.3 °C and the average low is 14.1 °C. Further meteorological characteristics of Perugia region with regards to the months of the present monitoring campaign, i.e. July and August, are tabulated in Table 4. July and August are generally reported as the warmest months of Perugia region. Moreover, July is reported as the sunniest, driest and least humid month of the year.

A.1. Incoming SR

In Fig. 12 the incident Global Solar Radiation (GSR) over the investigated fields is illustrated throughout the overall monitoring campaign. The values vary with respect to the time of the day. During the daytime, when the peaks in the corresponding curve occur, the incident global radiation typically exceeds 800 W/m2. The highest recorded value is 1160 W/m^2, while the average value is 296 W/m^2. For the purpose of the present analysis, three consequent (a) sunny and (b) cloudy days were identified for gauging the performance of the tested paving fields under different boundary conditions. The main criteria for distinguishing the monitored days as sunny and cloudy ones were the (i) proportion of the incident GSR in conjunction with (ii) the degree of the corresponding diurnal fluctuations. The three selected sunny days are the consequent days from 3rd to 5th of August with an average value of incoming solar radiation substantially exceeding the average value of the total cycle of the monitoring campaign. Additionally, almost no fluctuation can be observed for the incident GSR within these days and thus the sky can be considered as clear (Fig. 3). On the contrary, the selected three cloudy days, i.e. 27th–29th of July, present a lower average value than the corresponding average value of the monitoring period. Further on, as depicted in Fig. 3, fluctuations on the incoming GSR are constantly perceptible and thus the sky was substantially covered by clouds and in general characterized by weather instability.

Table 4
Meteorological characteristics of Perugia, Italy.

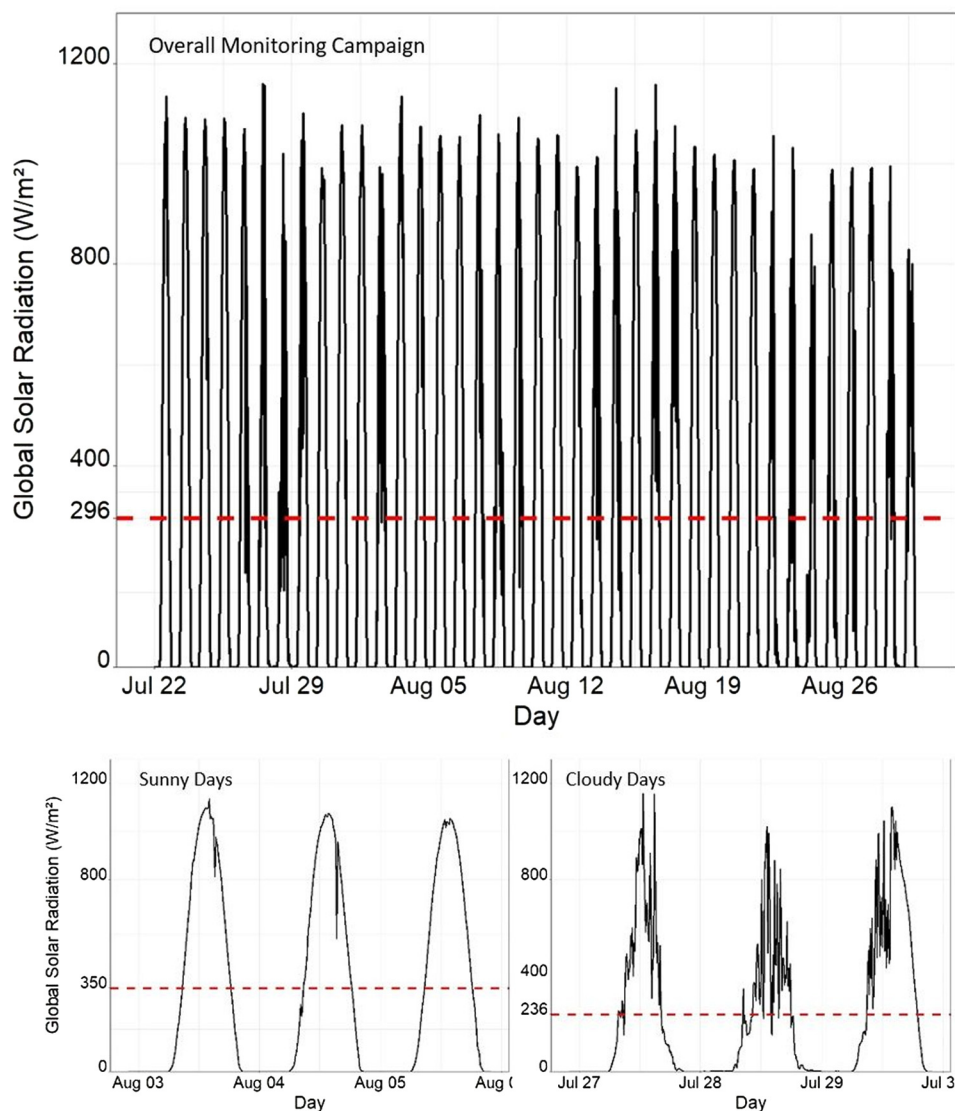|	July	August
Average T (°C)	22	22
Average T_{max} (°C)	30	29
Average T_{min} (°C)	15	15
Average precipitation (mm)	45	60
Probability of rain on a day (%)	16	16
Average sunlight hours/day	9 h 13'	8 h 11'
Average daylight hours/day	15 h 00'	13 h 54'

Fig. 12. Profiles during the monitoring campaign and selection of representative sunny and cloudy days.

References

Angelantoni Test Technologies, 2012. http://www.acstestchambers.com/Product/Prodotto?id_fam=1&id_prod=0.

ASTM, 2006. Standard test method for measuring solar reflectance of horizontal and low sloped surfaces in the field. ASTM E1918: 2006. American Society for Testing and Materials, West Conshohocken, PA.

ASTM, 2009. Standard test method for determination of solar reflectance near ambient temperature using a portable solar reflectometer. ASTM E1918: 2009. American Society for Testing and Materials.

Beck, Hylke E., Zimmermann, Niklaus E., McVicar, Tim R., Vergopolan, Noemi, Berg, Alexis, Wood, Eric F., 2018. Present and future Köppen-geiger climate classification maps at 1-km resolution. Sci. Data 5, 180214.

Berdahl, Paul, Akbari, Hashem, Levinson, Ronnen, Miller, William A., 2008. Weathering of roofing materials – an overview. Constr. Build. Mater. 22 (4), 423–433.

Berdahl, Paul, Chen, Sharon S., Destaillats, Hugo, Kirchstetter, Thomas W., Levinson, Ronnen M., Zalich, Michael A., 2016. Fluorescent cooling of objects exposed to sunlight – the ruby example. Sol. Energy Mater. Sol. Cells 157, 312–317.

Castaldo, V.L., Coccia, V., Cotana, F., Pignatta, G., Pisello, A.L., Rossi, F., 2015. Thermal-energy analysis of natural "cool" stone aggregates as passive cooling and global warming mitigation technique. Urban Clim, 14, 301–314 (Cooling Heat Islands).

Ceroni, Paola, 2016. Design of phosphorescent organic molecules: old concepts under a new light. Chem 1 (4), 524–526.

Clinton, Nicholas, Gong, Peng, 2013. Modis detected surface urban heat islands and sinks: global locations and controls. Remote Sens. Environ. 134, 294–304.

Cosgrove, Ann, Berkelhammer, Max, 2018. Downwind footprint of an urban heat island on air and lake temperatures. npj Clim. Atmosp. Sci. 1 (1), 46.

Doulos, L., Santamouris, M., Livada, I., 2004. Passive cooling of outdoor urban spaces.

The role of materials. Sol. Energy 77 (2), 231–249.

EN 197-1, 2011. Cement - part 1: Composition, specifications and conformity criteria for common cements. Br. Stand.

EN 197-2, 2014. Cement - part 2: Conformity evaluation. Br. Stand.

EN 934-2, 2012. Admixtures for concrete, mortar and grout - part 2: Concrete admixtures - definitions, requirements, conformity, marking and labelling. Br. Stand.

Ferguson, Bruce K., 2005. Porous Pavements. CRC Press.

Fichera, Alberto, Inturri, Giuseppe, La Greca, Paolo, Palermo, Valentina, 2016. A model for mapping the energy consumption of buildings, transport and outdoor lighting of neighbourhoods. Cities 55, 49–60.

Garshasbi, Samira, Santamouris, Mat, 2019. Using advanced thermochromic technologies in the built environment: recent development and potential to decrease the energy consumption and fight urban overheating. Sol. Energy Mater. Sol. Cells 191, 21–32.

Gutiérrez, Elkin I., Colorado, Henry A., 2020. Development and characterization of a luminescent coating for asphalt pavements. In: Characterization of Minerals, Metals, and Materials. Springer, pp. 511–519.

Koc, Carlos Bartesaghi, Osmond, Paul, Peters, Alan, 2018. Evaluating the cooling effects of green infrastructure: a systematic review of methods, indicators and data sources. Sol. Energy 166, 486–508.

Kolokotsa, Dionysia – Denia, Giannariakis, Gerassimos, Gobakis, Kostas, Giannarakis, Giannis, Synnefa, Afroditi, Santamouris, Mat, 2018. Cool roofs and cool pavements application in Acharnes, Greece. Sustain. Cities Soc. 37, 466–474.

Kyriakodis, G.-E., Santamouris, M., 2018. Using reflective pavements to mitigate urban heat island in warm climates - results from a large scale urban mitigation project. Urban Climate 24, 326–339.

Li, H., Harvey, J., Kendall, A., 2013. Field measurement of albedo for different land cover materials and effects on thermal performance. Build. Environ. 59, 536–546.

Mathew, Aneesh, Sreekumar, Sreenu, Khandelwal, Sumit, Kumar, Rajesh, 2019. Prediction of land surface temperatures for surface urban heat island assessment over

chandigarh city using support vector regression model. Sol. Energy 186, 404–415.

Nurwanda, Atik, Honjo, Tsuyoshi, 2020. The prediction of city expansion and land surface temperature in Bogor city, Indonesia. Sustain. Cities Soc. 52, 101772.

Perugia, umbria climate and temperature. http://www.perugia.climatemps.com/.

Pisello, A.L., Castaldo, V.L., Piselli, C., Fabiani, C., Cotana, F., 2017. Thermal performance of coupled cool roof and cool Façade: experimental monitoring and analytical optimization procedure. Energy Build. 157, 35–52.

Praticò, F.G., Vaiana, R., Noto, S., 2018. Photoluminescent road coatings for open-graded and dense-graded asphalts: theoretical and experimental investigation. J. Mater. Civ. Eng. 30 (8), 04018173.

Pyrgou, Andri, Castaldo, Veronica Lucia, Pisello, Anna Laura, Cotana, Franco, Santamouris, Mattheos, 2017. On the effect of summer heatwaves and urban overheating on building thermal-energy performance in central Italy. Sustain. Cities Soc. 28, 187–200.

Qin, Yinghong, 2015a. A review on the development of cool pavements to mitigate urban heat island effect. Renew. Sustain. Energy Rev. 52, 445–459.

Qin, Yinghong, 2015b. Urban canyon albedo and its implication on the use of reflective cool pavements. Energy Build. 96, 86–94.

Qin, Yinghong, Hiller, Jacob E., 2014. Understanding pavement-surface energy balance and its implications on cool pavement development. Energy Build. 85, 389–399.

Qin, Yinghong, Luo, Ju, Chen, Zheng, Mei, Guoxiong, Yan, Li-E, 2018. Measuring the albedo of limited-extent targets without the aid of known-albedo masks. Sol. Energy 171, 971–976.

Radulovic, Dusko, Skok, Srdjan, Kirincic, Vedran, 2011. Energy efficiency public lighting management in the cities. Energy 36(4), 1908–1915 (5th Dubrovnik Conference on Sustainable Development of Energy, Water Environment Systems).

Rosso, Federica, Pisello, Anna, Castaldo, Veronica, Ferrero, Marco, Cotana, Franco, 2017. On innovative cool-colored materials for building envelopes: balancing the architectural appearance and the thermal-energy performance in historical districts. Sustainability 9 (12), 2319.

Roth, Matthias, 2000. Review of atmospheric turbulence over cities. Quart. J. Roy. Meteorol. Soc. 126 (564), 941–990.

Santamouris, M., 2013. Using cool pavements as a mitigation strategy to fight urban heat island—a review of the actual developments. Renew. Sustain. Energy Rev. 26, 224–240.

Santamouris, M., Gaitani, N., Spanou, A., Saliari, M., Giannopoulou, K., Vasilakopoulou, K., Kardomateas, T., 2012. Using cool paving materials to improve microclimate of urban areas – design realization and results of the flisvos project. Build. Environ. 53, 128–136.

Santamouris, M., Ding, L., Fiorito, F., Oldfield, P., Osmond, Paul, Paolini, R., Prasad, D., Synnefa, A., 2017. Passive and active cooling for the outdoor built environment – analysis and assessment of the cooling potential of mitigation technologies using performance data from 220 large scale projects. Sol. Energy 154, 14–33 (Solar Thermal Heating and Cooling).

Steeneveld, G.J., Koopmans, S., Heusinkveld, B.G., Theeuwes, N.E., 2014. Refreshing the role of open water surfaces on mitigating the maximum urban heat island effect. Landscape Urban Plan. 121, 92–96.

Ulpiani, Giulia, 2019. Water mist spray for outdoor cooling: a systematic review of technologies, methods and impacts. Appl. Energy 254, 113647.

Vardoulakis, E., Karamanis, D., Fotiadi, A., Mihalakakou, G., 2013. The urban heat island effect in a small mediterranean city of high summer temperatures and cooling energy demands. Sol. Energy 94, 128–144.

Walter, Edward, Gibson, Oliver, 2020. The efficacy of antibiotics in reducing morbidity and mortality from heatstroke – a systematic review. J. Therm. Biol. 88, 102509.

World Bank, 2018. World development indicators - urban population. https://data.worldbank.org/indicator/SP.URB.TOTL.IN.ZS (accessed: 2018).

Yun, Geun Young, Ngarambe, Jack, Duhirwe, Patrick Nzivugira, Ulpiani, Giulia, Paolini, Riccardo, Haddad, Shamila, Vasilakopoulou, Konstantina, Santamouris, Mat, 2020. Predicting the magnitude and the characteristics of the urban heat island in coastal cities in the proximity of desert landforms. The case of Sydney. Sci. Total Environ. 709, 136043.

Zhu, Shanshan, Mai, Xianmin, 2019. A review of using reflective pavement materials as mitigation tactics to counter the effects of urban heat island. Adv. Compos. Hybrid Mater. 1–8.